Supplemental Material - Shear-Induced Heterogeneity in Associating Polymer Gels: Role of Network Structure and Dilatancy

Ahmad K. Omar and Zhen-Gang Wang*
Division of Chemistry and Chemical Engineering,
California Institute of Technology, Pasadena, CA 91125, USA

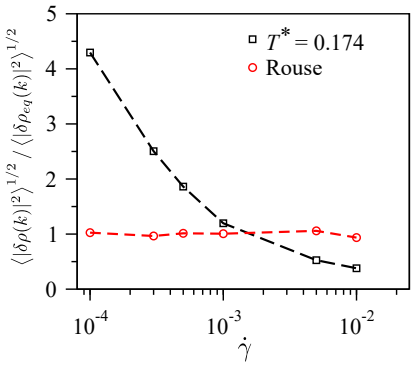

FIG. S1. Magnitude of the density heterogeneity at $k = 2\pi/L_z$ for an AP at $T^* = 0.174$ and for the Rouse solution. The subscript eq denotes equilibrium properties.

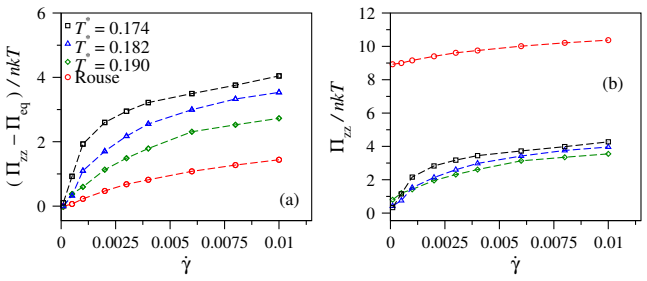

FIG. S2. (a) $(\Pi_{zz} - \Pi_{eq})/nkT$ and (b) Π_{zz}/nkT as a function of $\dot{\gamma}$ for gels of various T^* and Rouse system.

Equilibration. To reach the equilibrium state, for each ϵ_{ss} the sample is annealed at a reduced temperature $T^* = 1$ for a duration of $12\tau_R$, followed by quenching to $T^* = 1/\epsilon_{ss}$ over a period of $20\tau_R$. We then further equilibrate each sample for $95\tau_R$. The quiescent-state data (e.g. the osmotic pressure, diffusivity, and structural properties) are collected over a period of $190\tau_R$.

Methods. We compute stress using the well known Irving-Kirkwood expression $\boldsymbol{\sigma} = -\rho\langle\dot{\boldsymbol{r}}'\dot{\boldsymbol{r}}'\rangle - \rho\langle\boldsymbol{r}\boldsymbol{f_p}\rangle$ where $\langle\cdots\rangle$ denotes an average over all beads and $\dot{\boldsymbol{r}}' = \dot{\boldsymbol{r}} - \boldsymbol{r}\cdot\boldsymbol{\nabla v}_s$ represents velocity fluctuations (recall $m = 1$; the first term in the stress tensor simply results in $-\rho kT$). The particle (or osmotic) pressure is $\Pi = -\mathrm{tr}\boldsymbol{\sigma}/3$. The long-time self-diffusivity is measured from the chain center-of-mass mean-square-displacement $D = \lim_{t\to\infty}\frac{1}{6}D\left\langle(\Delta\boldsymbol{r}_{cm})^2\right\rangle/dt$. In presenting spatial profiles (see Fig. 2 in the main text), we shift the particles from each sample such that the concentrated band is at the bottom of the simulation box.

Structure Factor. To compute the magnitude of the density heterogeneity, we bin the simulation box in the gradient direction into 10 layers ($i = 1, 2, ..., 10$) of equal thickness and compute $\delta\rho(z_j) = \rho(z_j) - \bar{\rho}$. We then take a discrete spatial Fourier transform $\delta\rho(k) = \frac{1}{10}\sum_{j=1}^{10}\delta\rho(z_j)e^{ikz_j}$, reporting the ensemble (time and sample) averaged $\left\langle|\delta\rho(k)|^2\right\rangle = \langle\delta\rho(k)\delta\rho(-k)\rangle$. We use the density profiles obtained over the last $60\tau_R$ of shear (where little transience is observed) in computing $\delta\rho(z_j)$. The resulting coarse-grained structure factors (for both the Rouse solution and AP at $T^* = 0.174$) as a function of shear are shown in Fig. S1.

In our system, as we approach the unstable region (from higher shear rates) we find significant increases in the long wavelength ($k = 2\pi/L_z$) value of the structure factor – the magnitude of the density heterogeneity is greatly enhanced (relative to equilibrium) for $\dot{\gamma} < \dot{\gamma}^*$, and is suppressed for $\dot{\gamma} > \dot{\gamma}^*$.

Pressure. In the main text (see Fig. 3(a)), we show the deviatoric polymer pressure as a function of T^* and $\dot{\gamma}$ normalized by the equilibrium osmotic pressure Π_{eq} at the given T^*, in order to highlight the variation with respect to the quiescent-state value. Here, we normalize the deviatoric pressure by nkT to show the actual value in the pressure variation with shear. We also provide the actual values of the pressure itself in Fig. S2(b). As noted in the main text, at low $\dot{\gamma}$, the degree of dilation for AP gels can be significantly larger than for a Rouse solution, with APs at lower T^* exhibiting the largest pressure increases. While only the initial rapid variations in Π_{zz} with $\dot{\gamma}$ are relevant in the context of SCC (see main text), we note that Π_{zz} for all AP gels at a given $\dot{\gamma}$ are quite comparable.

Chain Conformation. To characterize the role of chain elasticity in stress generation we compute the radius of gyration $R_g^2 = \frac{1}{N}\sum_{i=1}^{N}(\boldsymbol{r}_i - \boldsymbol{r}_{cm})^2$ for each chain and report the average over all chains as a function of $\dot{\gamma}$ (for homogeneous flow) in Fig. S3. As noted in the main text, R_g for the AP chains in the z direction is less compressed than the corresponding Rouse system for all the $\dot{\gamma}$ explored. We note that at moderate shear rates the AP chains actually expand slightly, a direct consequence of the reduction of intramolecular association. While AP gels have a larger stress than the Rouse solution for all $\dot{\gamma}$, the relative AP chain extension in the x direction can be less than that of the Rouse solution. This observation

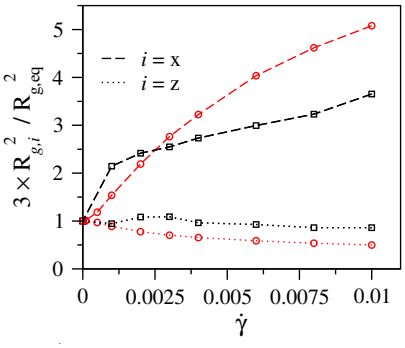

FIG. S3. The relative degree of chain extension in the flow (x) and gradient (z) directions for AP gel at $T^* = 0.174$ (□) and the Rouse solution (○) for $\dot{\gamma}$ in which the flow is homogeneous.

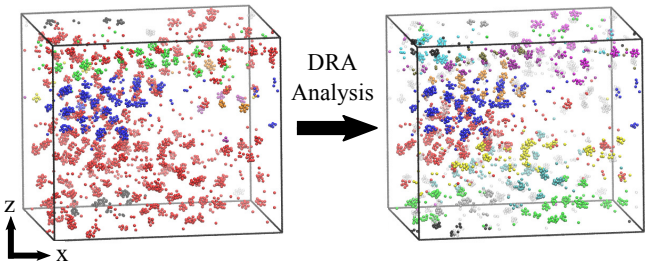

FIG. S4. Trimming of the AP gel network at $T^* = 0.174$ and $\dot{\gamma} = 10^{-2}$ with the DRA analysis.

suggests interesting behavior in the force-extension curve of APs.

Connectivity. Figure S4 contrasts the aggregates defined without and with applying the connectivity criteria (DRA) used in the main text. Even at the largest shear rates of $\dot{\gamma} = 10^{-2}$, including low-coordination clusters in defining aggregates results in a majority of the chains being included within a single space-spanning structure. Upon defining the DRAs, the space-spanning aggregate is broken up into several smaller aggregates.